Fault Location Method for Overhead Feeders with Distributed Generation Units Based on Direct Load Flow Approach

Charalampos G. Arsoniadis and Vassilis C. Nikolaidis, *Senior Member*, *IEEE*

***Abstract*—This paper proposes a novel fault location method for overhead feeders, which is based on the direct load flow approach. The method is developed in the phase domain to effectively deal with unbalanced network conditions, while it can also handle distributed generation (DG) units of any type without requiring equivalent models. By utilizing the line series parameters and synchronized or unsynchronized voltage and current phasor measurements taken from the sources, the method reliably identifies the most probable faulty sections. With the aid of an index, the exact faulty section among the multiple candidates is determined. Extensive simulation studies for the IEEE 123-bus test feeder demonstrate that the proposed method accurately estimates the fault position under numerous short-circuit conditions with varying pre-fault system loading conditions, fault resistances, and measurement errors. The proposed method is promising for practical applications due to the limited number of required measurement devices as well as the short computation time.**

***Index Terms*—Fault location, distribution system, direct load flow, distributed generation.**

I. Introduction

THE automated and precise localization of short-circuit faults in power distribution systems reduces the power supply restoration time, thus increasing the system reliability. In this regard, several methods have been developed so far for automated fault location in power distribution systems. In this paper, we apply the phasor-based fault location principle to develop an automated method which utilizes fundamental frequency phasors, extracted from signals measured from the field, and performs short-circuit theory calculations to estimate the exact fault distance.

The phasor-based fault location methods can be classified into bus-oriented [1]-[10] and branch-oriented [11]-[20] methods. The bus-oriented methods apply appropriate short-circuit fault calculations based on the classical bus impedance matrix ($\boldsymbol{Z}_{\text{bus}}$) theory. The branch-oriented methods apply several modifications of the three-phase power flow algorithm to find equivalent load impedances at different buses, which are then used to calculate the fault quantities and estimate the fault distance. Typically, for radial feeders, the backward/forward sweep load flow (BFSLF) algorithm is applied [21], [22].

In this paper, the direct load flow (DLF) approach [23] is modified to form a novel branch-oriented fault location method for radial overhead feeders with distributed generation (DG) units of any type, by using synchronized or unsynchronized measurements taken from the source buses. The DLF approach requires only the series impedance parameters of the line elements. Since overhead feeders do not have large capacitance to earth and the lengths of segments are relatively small, this assumption helps significantly improve the computation time of the proposed method. Moreover, DG units are handled as current injections. Hence, their models are not included in the mathematical formulation. Compared with the BFSLF algorithm, the proposed method does not require new data formatting/searching procedures; hence, the preparation and computation time is significantly reduced.

The proposed method identifies the exact fault location among the multiple estimates by using an error index for each candidate faulty section. The idea for this index originates in [24], but in this paper, the existence of DG units is also considered in the calculations. Moreover, in this paper, the equivalent load impedance of each bus required for the calculation of the index is simply determined by utilizing the modified DLF method, while in [24], complex computations are performed.

By comparing the proposed method with those in [1]-[20], the differences in Table I arise. Note that in Table I, CIDG stands for converter-interfaced DG; BU stands for bus-oriented fault location method; BR stands for branch-oriented fault location method; M stands for match rules for estimating the faulty bus; A is the analytical expression for estimating the faulty bus; A* is the analytical expression for estimating the exact fault location; abc stands for three-phase; M/S stands for multiple measurements (synchronized); M/U stands for multiple measurements (unsynchronized); M/S+U stands for multiple measurements (synchronized and unsynchronized); L/S stands for limited measurements (synchronized); L/U

Manuscript received: June 2, 2023; revised: September 29, 2023; accepted: December 25, 2023. Date of CrossCheck: December 25, 2023. Date of online publication: January 11, 2024.

The research work was supported by the Hellenic Foundation for Research and Innovation (HFRI) under the HFRI Ph.D. Fellowship grant (No. 1156).

C. G. Arsoniadis and V. C. Nikolaidis (corresponding author) are with the Department of Electrical and Computer Engineering, Democritus University of Thrace, Xanthi 67100, Greece (e-mail: carsonia@ee.duth.gr; vnikolai@ee.duth.gr).

DOI: 10.35833/MPCE.2023.000379

stands for limited measurements (unsynchronized); 2/S means that measurements from only 2 network points (locations) are required and these measurements must be synchronized; 1/- means that measurements from only 1 network point (location) are required; RL stands for resistor-inductor; and RLC stands for resistor-inductor-capacitor.

TABLE I
COMPARATIVE REVIEW OF DIFFERENT METHODS

Reference	Evaluation aspect							
	Type	Method	System	Rotating DG	CIDG	Measurement (points/type)	Line model	Multiple estimation
[1]	BU	A*	abc	Yes	No	L/S	RL	No
[2]	BU	A*	abc	Yes	No	2/S	RL	No
[3]	BU	M	abc	Yes	No	M/S	RL	No
[4]	BU	M	abc	Yes	No	M/S+U	RL	Yes
[5]	BU	M	abc	No	No	M/S	RL	No
[6]	BU	A	abc	Yes	Yes	M/U	RL	No
[7]	BU	A*	abc	Yes	Yes	L/S	RLC	Yes
[8]	BU	A*	abc	Yes	Yes	L/U	RLC	Yes
[9]	BU	A*	abc	Yes	Yes	L/S	RLC	Yes
[10]	BU	A*	abc	Yes	Yes	M/S	RLC	Yes
[11]	BR	A*	abc	Yes	Yes	L/S	RLC	No
[12]	BR	A*	abc	No	No	1/-	RLC	No
[13]	BR	A*	abc	No	No	1/-	RL	Yes
[14]	BR	A*	abc	No	No	1/-	RL	No
[15]	BR	A*	abc	Yes	Yes	L/S	RLC	No
[16]	BR	A*	abc	No	Yes	1/-	RLC	No
[17]	BR	A*	abc	Yes	Yes	L/U	RL	No
[18]	BR	M	abc	No	No	M/S	RL	No
[19]	BR	A*	abc	Yes	Yes	L/S	RLC	No
[20]	BR	M	abc	Yes	Yes	M/S	RLC	Yes
This paper	BR	A*	abc	Yes	Yes	L/S	RL	Yes

The contributions of this paper are summarized below.

1) The DLF approach [23] is for the first time used in fault location. For this purpose, we have modified it to handle both synchronized or unsynchronized measurements and find the possible faulty sections.

2) A modified formulation of the error index with respect to that originally proposed in [24] is made in this paper as part of the algorithm for elimination of multiple fault location estimations. The elimination of multiple solutions is not dealt with at all in [1]-[3], [5], [6], [11], [12], [14]-[17].

3) The proposed method can be equally applied to distribution systems with any type of DG units, i.e., synchronous-machine-based DG units and/or CIDG units, since the DG unit model is not required in the calculations. References [5], [12]-[14], and [18] do not consider DG units at all, whereas [1]-[4] consider DG units by adopting a simplified voltage source behind an equivalent impedance model.

4) A limited number of synchronized or unsynchronized measurements taken from the source buses are required. On the contrary, the methods in [3]-[6], [10], [18], and [20] require measurements from a large number of buses, whereas [3]-[5] strictly depend on synchronized measurements.

The structure of this paper is organized as follows. Section II gives the formulation of the fault location problem. The proposed method is thoroughly described in Section III. Section IV explains how unsynchronized phasors are handled properly. Section V presents the method for eliminating multiple solutions to identify the real faulty section among multiple candidates. Section VI gives an insight of how the method can be implemented in real-world feeders. Section VII presents the fault location results. Comparison with other fault location methods is conducted in Section VIII. Finally, Section IX concludes this paper.

II. FORMULATION OF FAULT LOCATION PROBLEM

Typically, most branch-oriented fault location methods for active distribution networks involve three discrete development stages: ① the derivation of the fault location equation, ② the calculation of the sending-end quantities of each successive line section, and ③ the estimation of the fault current contribution from the feeder area that is downstream to the fault position. These stages are analyzed below with respect to how they are realized by relevant fault location methods, in order to highlight the contribution of this paper.

A. Derivation of Fault Location Equation

Consider a purely resistive three-phase fault at distance d from the sending-end s of line section s-r, as shown in Fig. 1. The fault divides line section s-r into the subsections s-f and f-r. PS stands for power station.

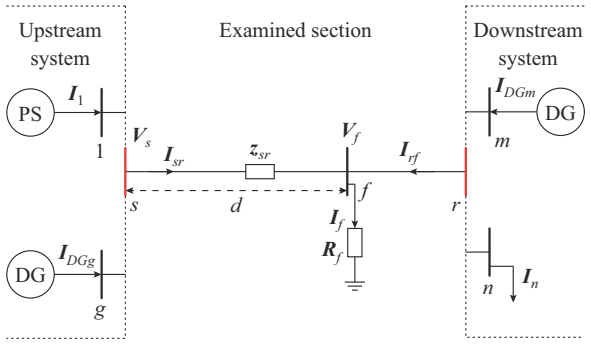

Fig. 1. Examined line section s-r.

If the short-line model is used for representing each subsection, the voltage vector $\boldsymbol{V}_f=[V_{fa}, V_{fb}, V_{fc}]^{\mathrm{T}}$ (a, b, and c are three phases) at the fault position is expressed by the following matrix equation:

$$\boldsymbol{V}_f=\boldsymbol{V}_s-d\boldsymbol{z}_{sr}\boldsymbol{I}_{sr} \tag{1}$$

where $\boldsymbol{V}_s=[V_{sa}, V_{sb}, V_{sc}]^{\mathrm{T}}$ is the voltage vector at the sending-end s of line section s-r; $\boldsymbol{I}_{sr}=[I_{sra}, I_{srb}, I_{src}]^{\mathrm{T}}$ is the current vector of line section s-r; and $\boldsymbol{z}_{sr}$ is the series impedance matrix.

The three-phase apparent power at the fault position is given by:

$$\boldsymbol{S}_f=\boldsymbol{V}_f^{\mathrm{T}}\boldsymbol{I}_f^{*}=(\boldsymbol{R}_f\boldsymbol{I}_f)^{\mathrm{T}}\boldsymbol{I}_f^{*} \tag{2}$$

where $\boldsymbol{R}_f$ is a 3×3 fault resistance vector; $\boldsymbol{I}_f=[I_{fa}, I_{fb}, I_{fc}]^{\mathrm{T}}$ is the fault current vector; and "*" denotes the conjugate of the current.

By combining (1) and (2), the following fault location equation is derived:

$$d = \frac{\mathrm{Im}(\boldsymbol{V}_s^{\mathrm{T}} \boldsymbol{I}_f^*)}{\mathrm{Im}(\boldsymbol{I}_{sr}^{\mathrm{T}} \boldsymbol{z}_{sr}^{\mathrm{T}} \boldsymbol{I}_f^*)} \tag{3}$$

where Im(·) defines the imagine part of a complex number.

If the π-line model is used for representing subsections *s-f* and *f-r*, the voltage at the fault location is given by:

$$\boldsymbol{V}_f = \boldsymbol{D}(d)\boldsymbol{V}_s - \boldsymbol{B}(d)\boldsymbol{I}_{sr} \tag{4}$$

$$\boldsymbol{B}(d) = d\boldsymbol{z}_{sr} \tag{5}$$

$$\boldsymbol{D}(d) = \boldsymbol{U} + 0.5d^2 \boldsymbol{z}_{sr}\boldsymbol{y}_{sr} \tag{6}$$

where $\boldsymbol{U}$ is a 3×3 unit matrix; and $\boldsymbol{y}_{sr}$ is the series admittance matrix of line section *s-r*.

By combining (2) and (4), the quadratic fault location equation is derived as:

$$\boldsymbol{a}_2 d^2 + \boldsymbol{a}_1 d + \boldsymbol{a}_0 = \boldsymbol{0} \tag{7}$$

$$\boldsymbol{a}_2 = \mathrm{Im}(0.5\boldsymbol{V}_s^{\mathrm{T}} \boldsymbol{z}_{sr}\boldsymbol{y}_{sr}\boldsymbol{I}_f^*) \tag{8}$$

$$\boldsymbol{a}_1 = \mathrm{Im}(-\boldsymbol{I}_{sr}^{\mathrm{T}} \boldsymbol{z}_{sr}\boldsymbol{I}_f^*) \tag{9}$$

$$\boldsymbol{a}_0 = \mathrm{Im}(\boldsymbol{V}_s^{\mathrm{T}} \boldsymbol{I}_f^*) \tag{10}$$

Equation (3) is utilized in [17] and (7) is utilized in [7], [11], [12], [15] for determining the fault distance inside a line section. However, a different method for estimating the unknown quantities is used in both alternatives. The details of those different methods are addressed in the following two subsections.

B. Calculation of Sending-end Quantities

For each examined line section, both alternative fault location equations, i.e., (3) and (7), require the sending-end voltage and current to calculate the fault distance. For the first line section of a feeder, which departs from the main substation, these quantities are known from available voltage/current measurements. This is because measurement devices are always available at the substation. For all the remaining line sections, the sending-end voltage and current are calculated by using the measurements taken at the substation.

In [11]-[14], this procedure is executed manually, through an iterative search process in the part of the feeder upstream to the fault position. This method is not feasible in cases of large feeders with many (sub)laterals and intermediate loads. Instead, in [15]-[17], the BFSLF algorithm is applied to the feeder that is upstream to the fault. The BFSLF algorithm requires only the voltage at the head of the feeder and estimates the line currents and bus voltages of the remaining system. A different method is applied in [6], where a reduced version of the original $\boldsymbol{Z}_{\mathrm{bus}}$ is used, reflecting the upstream part of the system.

C. Estimation of Fault Current Contribution from Downstream System

In order to solve (3) or (7), except from the sending-end quantities, the knowledge of the fault current $\boldsymbol{I}_f$ is required. The latter is given from the following equation:

$$\boldsymbol{I}_f = \boldsymbol{I}_{sr} + \boldsymbol{I}_{rf} \tag{11}$$

The sending-end current $\boldsymbol{I}_{sr}$ is calculated as described in the previous subsection. Therefore, the only unknown in (11) is the current $\boldsymbol{I}_{rf}$ flowing from the downstream system to the fault.

If DG units are absent in the area downstream to the fault position, the current $\boldsymbol{I}_{rf}$ is the during-fault load current $\boldsymbol{I}_{fr}^{load}$. The latter has the opposite direction with respect to $\boldsymbol{I}_{rf}$, i.e.,

$$\boldsymbol{I}_{rf} = -\boldsymbol{I}_{fr}^{load} \tag{12}$$

Since the pre-fault load current is different from the during-fault load current $\boldsymbol{I}_{fr}^{load}$, the latter is estimated in an iterative manner. This procedure requires the calculation of the equivalent circuit of the downstream feeder, as can be observed from the end-bus of each examined line section. In [12], the equivalent circuit is obtained by equivalencing all the series and parallel elements of the downstream system. It is obvious that this method is not suitable for large distribution systems, and it can hardly be applied in practical applications. Instead, the BFSLF algorithm is used in [13] and [14] to obtain the equivalent circuits. However, the aforementioned papers do not consider DG sources.

If DG units are operating in the downstream system, the current $\boldsymbol{I}_{rf}$ expresses the net remote infeed from those units during the fault:

$$\boldsymbol{I}_{rf} = \sum_i \boldsymbol{I}_{DGi} - \boldsymbol{I}_{fr}^{load} \tag{13}$$

where i is the number of DG units connected downstream to the fault position; and $\boldsymbol{I}_{DGi}$ is the current contribution of each of those DG units to the fault.

In [15]-[17], the remote fault current contribution is estimated by applying the BFSLF algorithm in the downstream system, where the DG sources are handled as current injections. In [6], the reduced bus impedance matrix of the downstream system is used for estimating the infeed current $\boldsymbol{I}_{rf}$.

III. Proposed Fault Location Method

In this paper, we propose a fault location method by solving (3) (due to the short-line model adopted) for locating the fault inside a line section of a distribution feeder. Contrary to most of the relevant methods published in the literature, which apply the BFSLF algorithm for estimating the sending-end quantities and the remote infeed current, we apply a modified DLF approach [23] for this purpose.

A. DLF Approach

The DLF approach directly updates and recalculates the branch currents and bus voltages by utilizing the bus-injection-to-branch-current matrix ***BIBC*** and branch-current-to-bus-voltage matrix ***BCBV***, respectively [23]. ***BIBC*** and ***BCBV*** are explained with the sample 4-bus power distribution network shown in Fig. 2.

The branch currents of this power distribution network can be expressed by the bus current injections, as shown in (14), where the upper triangular transformation matrix of 0 and 1 values is the ***BIBC*** matrix. Note that in (14), the branch/bus currents correspond to a 3×1 vector each, since all three phases are considered.

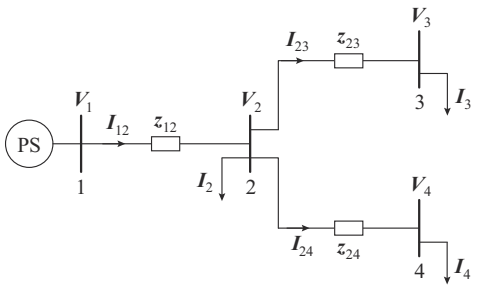

Fig. 2. Sample 4-bus power distribution network.

$$\begin{bmatrix} \boldsymbol{I}_{12} \\ \boldsymbol{I}_{23} \\ \boldsymbol{I}_{24} \end{bmatrix} = \begin{bmatrix} 1 & 1 & 1 \\ 0 & 1 & 0 \\ 0 & 0 & 1 \end{bmatrix} \begin{bmatrix} \boldsymbol{I}_2 \\ \boldsymbol{I}_3 \\ \boldsymbol{I}_4 \end{bmatrix} \Rightarrow \boldsymbol{I}_{ij} = \boldsymbol{BIBC} \cdot \boldsymbol{I}_j \tag{14}$$

where $\boldsymbol{I}_{ij}$ is the current flow on branch ij; and $\boldsymbol{I}_j$ is the load current supplied from bus j. The drop between the substation bus voltage and the voltage of each downstream bus is calculated through (15), where the lower triangular matrix is ***BCBV*** containing only the series impedance of the lines.

$$\begin{bmatrix} \boldsymbol{V}_1 - \boldsymbol{V}_2 \\ \boldsymbol{V}_1 - \boldsymbol{V}_3 \\ \boldsymbol{V}_1 - \boldsymbol{V}_4 \end{bmatrix} = \begin{bmatrix} z_{12} & 0 & 0 \\ z_{12} & z_{23} & 0 \\ z_{12} & 0 & z_{24} \end{bmatrix} \begin{bmatrix} \boldsymbol{I}_{12} \\ \boldsymbol{I}_{23} \\ \boldsymbol{I}_{24} \end{bmatrix} \Rightarrow \Delta \boldsymbol{V}_{1j} = \boldsymbol{BCBV} \cdot \boldsymbol{I}_{ij} \tag{15}$$

where $\Delta \boldsymbol{V}_{1j} = \boldsymbol{V}_1 - \boldsymbol{V}_j$ is the voltage drop between bus 1 and bus j; and z_{ij} is the series impedance of line ij. The advantage of using the ***BIBC*** matrix is that branch current variations, caused by bus current variations, are calculated directly through (14); whereas in the BFSLF algorithm, multiple backward sweeps (equal to the number of line sections) are executed for the same purpose. With the use of the ***BCBV*** matrix, the voltage differences are calculated in one step through (15). In contrast, the BFSLF algorithm calculates the voltage differences, each at a time, by applying forward sweeps.

By combining (14) with (15), the following equation is derived:

$$\Delta \boldsymbol{V}_{1j} = \boldsymbol{BCBV} \cdot \boldsymbol{BIBC} \cdot \boldsymbol{I}_j = \boldsymbol{DLF} \cdot \boldsymbol{I}_j \tag{16}$$

Equation (16) relates bus currents with bus voltages, through the ***DLF*** matrix, as an alternative to the original bus impedance matrix $\boldsymbol{Z}_{\text{bus}}$. The difference between those matrices is that ***DLF*** includes only the series impedances of the line sections.

In the next subsections, we present how the DLF approach is modified in this paper so that it can be separately applied to determine the sending-end quantities and the receiving-end during-fault current contribution for the upstream and downstream systems, respectively.

B. DLF in Upstream System to Determine $\boldsymbol{V}_s$ and $\boldsymbol{I}_{sr}$

Let us consider the sample distribution feeder shown in Fig. 3, which is subject to a fault at point f of line section s-r. The first line section (i.e., section 1-2) departs from the main substation, where voltages and currents are measured from voltage and current transformers, respectively, which are always available in the field. Hence, the sending-end voltage vector $\boldsymbol{V}_1$ and the sending-end current vector $\boldsymbol{I}_{12}$ for line section 1-2 are known (measured) quantities, respectively, i.e., $\boldsymbol{V}_1 = \boldsymbol{V}_1^{meas}$, $\boldsymbol{I}_{12} = \boldsymbol{I}_1^{meas}$. For each other line section, e.g., for line section s-r, the corresponding during-fault sending-end voltage and current quantities, i.e., $\boldsymbol{V}_s$ and $\boldsymbol{I}_{sr}$, respectively, are calculated by applying the DLF approach for the network part upstream to bus s.

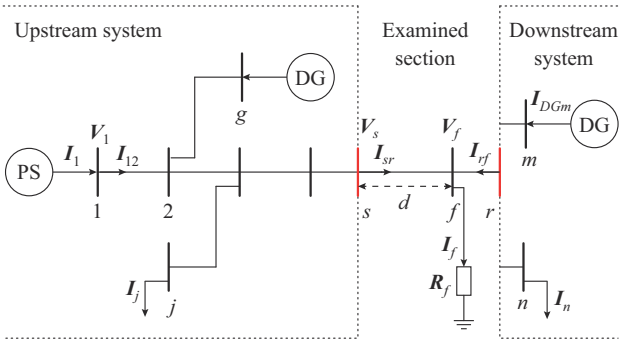

Fig. 3. Upstream system consideration.

The procedure adopted includes the following steps.

Step 1: formulate the matrices $\boldsymbol{BIBC}_{1\text{-}s}$ and $\boldsymbol{BCBV}_{1\text{-}s}$ for the network part from bus 1 down to bus s.

Step 2: if a DG unit is connected to bus g in the upstream network with respect to the fault point ($g < s$), set the during-fault bus current injection $\boldsymbol{I}_g$ to be equal to the measured current at the DG bus $\boldsymbol{I}_{DGg}^{meas}$.

$$\boldsymbol{I}_g = -\boldsymbol{I}_{DGg}^{meas} \tag{17}$$

Step 3: formulate the during-fault voltage and current vector of all network buses $1, 2, \ldots, s$, which are located upstream to the examined line section s-r. The superscript $k = 0, 1, 2, \ldots$ is used in (18) and (19) because each upstream bus voltage/current, except for bus 1, will be calculated in an iterative manner in the next steps.

$$\boldsymbol{V}_{1\text{-}s}^k = \begin{bmatrix} \boldsymbol{V}_1^{meas} & \boldsymbol{V}_2^k & \ldots & \boldsymbol{V}_s^k \end{bmatrix}^{\mathrm{T}} \tag{18}$$

$$\boldsymbol{I}_{1\text{-}s}^k = \begin{bmatrix} \boldsymbol{I}_1^{meas} & \boldsymbol{I}_2^k & \ldots & \boldsymbol{I}_s^k \end{bmatrix}^{\mathrm{T}} \tag{19}$$

Step 4: depending on load type, define the during-fault bus (load) currents in the upstream system with appropriate expressions. For instance, if bus j ($j < s$) is considered, then:

$$\boldsymbol{I}_j^k = \begin{cases} \begin{bmatrix} (S_{ja}/V_{ja}^k)^* & (S_{jb}/V_{jb}^k)^* & (S_{jc}/V_{jc}^k)^* \end{bmatrix}^{\mathrm{T}} & \text{(CP)} \\ \begin{bmatrix} (V_{ja}^k/z_{ja})^* & (V_{jb}^k/z_{jb})^* & (V_{jc}^k/z_{jc})^* \end{bmatrix}^{\mathrm{T}} & \text{(CI)} \\ \begin{bmatrix} I_{ja} & I_{jb} & I_{jc} \end{bmatrix}^{\mathrm{T}} & \text{(CC)} \end{cases} \tag{20}$$

where CP, CI, and CC characterize the constant power, constant impedance, and constant current load, respectively; S_j is the per-phase complex power injected into bus j; and z_j is the per-phase impedance of the load connected to bus j.

Step 5: at the initial step ($k = 0$), set each bus voltage equal to the measured bus voltage $\boldsymbol{V}_1^{meas}$. In matrix form, we have:

$$\boldsymbol{V}_{1\text{-}s}^0 = \begin{bmatrix} \boldsymbol{V}_1^{meas} & \boldsymbol{V}_2^0 & \ldots & \boldsymbol{V}_s^0 \end{bmatrix}^{\mathrm{T}} = \begin{bmatrix} \boldsymbol{V}_1^{meas} & \boldsymbol{V}_1^{meas} & \ldots & \boldsymbol{V}_1^{meas} \end{bmatrix}^{\mathrm{T}} \tag{21}$$

Step 6: the matrix of the initially estimated during-fault bus currents flowing in the upstream network is derived from (20) by replacing the voltages with their initially estimated during-fault value (except for CC loads):

$$\boldsymbol{I}_{1\text{-}s}^{0}=\left[\boldsymbol{I}_{1}^{meas}\quad \boldsymbol{I}_{2}^{0}\quad \ldots\quad \boldsymbol{I}_{s}^{0}\right]^{\mathrm{T}} \tag{22}$$

Step 7: calculate the during-fault sending-end current of the examined section *s*-*r* as:

$$\boldsymbol{I}_{sr}^{k}=\boldsymbol{I}_{1}^{meas}+\sum\boldsymbol{I}_{DGg}^{meas}-\sum_{j=2}^{s}\boldsymbol{I}_{j}^{k}\quad k=0,1,2,\ldots \tag{23}$$

Step 8: update the bus voltage vector directly as:

$$\boldsymbol{V}_{1\text{-}s}^{k+1}=\boldsymbol{V}_{1\text{-}s}^{k}-\Delta\boldsymbol{V}_{1\text{-}s}^{k} \tag{24}$$

$$\Delta\boldsymbol{V}_{1\text{-}s}^{k}=\boldsymbol{BCBV}_{1\text{-}s}\cdot\boldsymbol{BIBC}_{1\text{-}s}\cdot\boldsymbol{I}_{1\text{-}s}^{k} \tag{25}$$

where $\Delta\boldsymbol{V}_{1\text{-}s}^{k}$ is the vector of voltage drop between the substation bus (bus 1) and each downstream bus (up to bus *s*).

Step 9: if $\boldsymbol{V}_{1\text{-}s}^{k+1}\approx\boldsymbol{V}_{1\text{-}s}^{k}$, report the calculated during-fault sending-end voltage $\boldsymbol{V}_{s}^{calc}=\boldsymbol{V}_{s}^{k+1}$ and current $\boldsymbol{I}_{sr}^{calc}=\boldsymbol{I}_{sr}^{k+1}$ of section *s*-*r*; else, go to *Step 3*.

C. DLF in Downstream System to Determine d and $\boldsymbol{I}_{rf}$

The receiving-end current $\boldsymbol{I}_{rf}$ is required to calculate the total fault current through (11). The current $\boldsymbol{I}_{rf}$ is estimated by applying the DLF approach for the network part downstream to pseudo-bus *f*, as shown in Fig. 4.

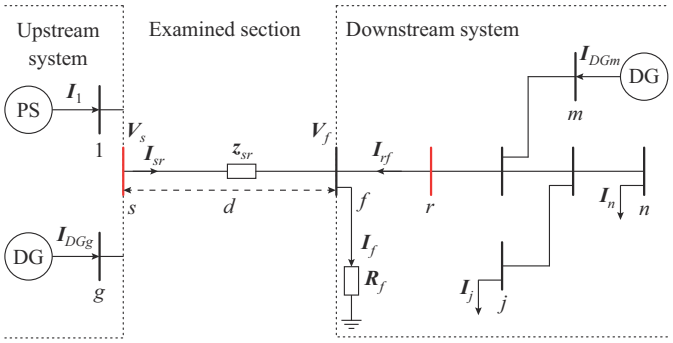

Fig. 4. Downstream system consideration.

This procedure includes the following steps.

Step 1: formulate the matrices $\boldsymbol{BIBC}_{f\text{-}n}$ and $\boldsymbol{BCBV}_{f\text{-}n}$ for the network part from pseudo-bus *f* down to the remotest bus *n*.

Step 2: if a DG unit is connected to bus *m* in the downstream system ($m>f$), set the during-fault bus current injection $\boldsymbol{I}_m$ equal to the measured current at the DG bus.

$$\boldsymbol{I}_{m}=-\boldsymbol{I}_{DG,m}^{meas} \tag{26}$$

Step 3: formulate the during-fault voltage and current vectors of all network buses $f, f+1, \ldots, n$, which are located downstream to the examined fault position.

$$\boldsymbol{V}_{f\text{-}n}^{k}=\left[\boldsymbol{V}_{f}^{k}\quad \boldsymbol{V}_{f+1}^{k}\quad \ldots\quad \boldsymbol{V}_{n}^{k}\right]^{\mathrm{T}} \tag{27}$$

$$\boldsymbol{I}_{f\text{-}n}^{k}=\left[\boldsymbol{I}_{f}^{k}\quad \boldsymbol{I}_{f+1}^{k}\quad \ldots\quad \boldsymbol{I}_{n}^{k}\right]^{\mathrm{T}} \tag{28}$$

Step 4: at the initial step ($k=0$), set the initial per unit fault distance estimation to be 0, i.e., $d^0=0$.

Step 5: calculate the fault point voltage $\boldsymbol{V}_{f}^{k}$ for d^k ($k=0, 1, 2, \ldots$) from the following equation:

$$\boldsymbol{V}_{f}^{k}=\boldsymbol{V}_{s}^{calc}-d^{k}\boldsymbol{z}_{sr}\boldsymbol{I}_{sr}^{calc} \tag{29}$$

where $\boldsymbol{V}_{s}^{calc}$ and $\boldsymbol{I}_{sr}^{calc}$ have been calculated as addressed in the previous subsection.

Step 6: set the initially estimated voltages of each downstream bus equal to the fault point voltage $\boldsymbol{V}_{f}^{0}$.

$$\boldsymbol{V}_{f\text{-}n}^{0}=\left[\boldsymbol{V}_{f}^{0}\quad \boldsymbol{V}_{f+1}^{0}\quad \ldots\quad \boldsymbol{V}_{n}^{0}\right]^{\mathrm{T}}=\left[\boldsymbol{V}_{f}^{0}\quad \boldsymbol{V}_{f}^{0}\quad \ldots\quad \boldsymbol{V}_{f}^{0}\right]^{\mathrm{T}} \tag{30}$$

Step 7: depending on the load type, calculate the initially estimated during-fault bus (load) currents through (20) using the bus voltages of (30).

Step 8: update the bus voltages directly as:

$$\boldsymbol{V}_{f\text{-}n}^{k+1}=\boldsymbol{V}_{f\text{-}n}^{k}-\Delta\boldsymbol{V}_{f\text{-}n}^{k} \tag{31}$$

$$\Delta\boldsymbol{V}_{f\text{-}n}^{k}=\boldsymbol{BCBV}_{f\text{-}n}\cdot\boldsymbol{BIBC}_{f\text{-}n}\cdot\boldsymbol{I}_{f\text{-}n}^{k} \tag{32}$$

Step 9: if $\boldsymbol{V}_{f\text{-}n}^{k+1}\approx\boldsymbol{V}_{f\text{-}n}^{k}$, calculate the branch currents directly from (33) and report the receiving-end current $\boldsymbol{I}_{rf}=-\boldsymbol{I}_{fr}$ as retrieved by (34); else, go to *Step 7*.

$$\boldsymbol{I}_{fr}^{k}=\boldsymbol{BIBC}_{f\text{-}n}\cdot\boldsymbol{I}_{r}^{k} \tag{33}$$

$$\boldsymbol{I}_{fr}^{k}=\boldsymbol{I}_{fr}^{k}(1,1) \tag{34}$$

Step 10: using the receiving-end current $\boldsymbol{I}_{fr}^{k}$, update the fault current $\boldsymbol{I}_{f}^{k}$ through:

$$\boldsymbol{I}_{f}^{k}=\boldsymbol{I}_{sr}^{calc}+\boldsymbol{I}_{rf}^{k} \tag{35}$$

Step 11: calculate the fault location from:

$$d^{k}=\frac{\mathrm{Im}\left((\boldsymbol{V}_{s}^{calc})^{\mathrm{T}}(\boldsymbol{I}_{f}^{k})^{*}\right)}{\mathrm{Im}\left((\boldsymbol{I}_{sr}^{calc})^{\mathrm{T}}\boldsymbol{z}_{sr}^{\mathrm{T}}(\boldsymbol{I}_{f}^{k})^{*}\right)} \tag{36}$$

Step 12: if $d^{k+1}\approx d^{k}$ and $0<d^{k+1}\le 1$, report the faulty section *s*-*r* and the fault distance; else, go to *Step 5*.

IV. Handling Unsynchronized Measurements

The proposed method requires voltage and current phasor measurements taken from the substation, and current phasor measurements taken from the DG units. For the sake of simplicity, these phasor measurements are considered synchronized in this section. In the general case where measurements are unsynchronized, the proposed method can still be applied but the power factor angles of the DG units are also required. This will be described in the rest of this section.

Assume the distribution feeder shown in Fig. 3. The substation bus 1 is taken as the reference bus. Therefore, its voltage angle is zero ($\delta_1=0$) and all other bus voltage angles are measured with respect to the reference angle.

To impose a synchronization error on the measured phasors (expressed by superscript "*err*"), we multiply these phasors with an exponential operator:

$$\begin{cases}\boldsymbol{V}_{1}^{err}=\boldsymbol{V}_{1}\mathrm{e}^{-\mathrm{j}0}\\ \boldsymbol{I}_{1}^{err}=\boldsymbol{I}_{1}\mathrm{e}^{-\mathrm{j}0}\end{cases} \tag{37}$$

$$\begin{cases}\boldsymbol{V}_{g}^{err}=\boldsymbol{V}_{g}\mathrm{e}^{-\mathrm{j}\delta_g}\\ \boldsymbol{I}_{DGg}^{err}=\boldsymbol{I}_{DGg}\mathrm{e}^{-\mathrm{j}\delta_g}\end{cases} \tag{38}$$

$$\begin{cases}\boldsymbol{V}_{m}^{err}=\boldsymbol{V}_{m}\mathrm{e}^{-\mathrm{j}\delta_m}\\ \boldsymbol{I}_{DGm}^{err}=\boldsymbol{I}_{DGm}\mathrm{e}^{-\mathrm{j}\delta_m}\end{cases} \tag{39}$$

As can be observed, besides currents measurement, the voltage measurements are also required for the DG units. Note that voltage and current measurements are always available in DG plants. Furthermore, we assume random error angles δ_g and δ_m for the measurements taken from the DG

units. We further assume that the measurements at substation (bus 1) are synchronized.

The power factor angles of DG units g and m are given by:

$$\varphi_g = angle(\boldsymbol{V}_g) - angle(\boldsymbol{I}_g) \tag{40}$$

$$\varphi_m = angle(\boldsymbol{V}_m) - angle(\boldsymbol{I}_m) \tag{41}$$

This angle separation is calculated from the voltage/current phasor measurements, reaching a relatively large value during faults. Note also that angles φ_g and φ_m are the same despite whether we assume the angle error in the voltage/current phasors or not.

The measured current phasors of the DG units can now be expressed as:

$$\boldsymbol{I}_{DGg}^{err} = \left| \boldsymbol{I}_{DGg} \right| e^{-j(\delta_g + \varphi_g)} \tag{42}$$

$$\boldsymbol{I}_{DGm}^{err} = \left| \boldsymbol{I}_{DGm} \right| e^{-j(\delta_m + \varphi_m)} \tag{43}$$

In (42) and (43), δ_g and δ_m are unknown quantities that will be estimated as explained below.

In the first iteration ($k=0$) of the fault location method described in Section III, we assume that $\delta_g = \delta_m = 0$. Then, the terms $\boldsymbol{I}_{DGg}^{err}$ and $\boldsymbol{I}_{DGm}^{err}$ are calculated and used in the algorithmic steps. In the next iterations ($k=1,2,3,\ldots$), δ_g and δ_m are updated using the new estimation of the DG bus voltages retrieved from (24) or (31):

$$\delta_g^k = angle(\boldsymbol{V}_g^k) \tag{44}$$

$$\delta_m^k = angle(\boldsymbol{V}_m^k) \tag{45}$$

It should be noted that φ_g and φ_m remain constant. Meanwhile, $\boldsymbol{V}_g$ and $\boldsymbol{V}_m$ are recalculated during the execution of the fault location algorithm until the condition of *Step 9* is satisfied. This is achieved when $\delta_i^{k+1} \approx \delta_i^k, i = g, m$.

V. Elimination of Multiple Solutions

A. Principle

By applying the proposed method to each line section successively, multiple acceptable fault distance estimation solutions may be obtained. Hence, multiple possible faulty sections may be identified. To deal with this problem, i.e., to identify the exact faulty section and the exact fault position inside this section, a fault distance estimation error index (FDEEI) is introduced:

$$FDEEI = \frac{0.5}{\left| d_m \right|} \sum_{e=1}^{2} \left| d_m - d_e \right| \tag{46}$$

where d_m and d_e are the fault distances estimated from the main and extra fault location equations (see Table II), respectively.

This index is based on the concept that extra linear independent fault location equations can be obtained from each phase (faulty and nonfaulty) if they are considered individually [24]. Based on this concept, the extra fault location equations of Table II are obtained by analyzing the sending-end voltage equation referring to the faulty section. Note that in Table II, AG, ABG, and ABCG stand for single-phase-to-ground, two-phase-to-ground, and three-phase-to-ground faults, respectively; and AB stands for phase-to-phase fault.

TABLE II
Extra Fault Location Equations

Fault type	Extra fault location equation 1	Extra fault location equation 2
AG	$\dfrac{\mathrm{Im}\left(\dfrac{V_a - V_b + V_c}{I_a} + B\dfrac{I_b}{I_a} + C\dfrac{I_c}{I_a}\right)}{\mathrm{Im}(z_{aa} - z_{ba} + z_{ca} + A)}$	$\dfrac{\mathrm{Im}\left(\dfrac{V_a + V_b - V_c}{I_a} - B\dfrac{I_b}{I_a} - C\dfrac{I_c}{I_a}\right)}{\mathrm{Im}(z_{aa} + z_{ba} - z_{ca} + A)}$
AB/ ABG	$\dfrac{\mathrm{Im}\left(\dfrac{V_a - V_b}{I_a - I_b}\right)}{\mathrm{Im}\left(\dfrac{DI_a + EI_b + FI_c}{I_a - I_b}\right)}$	$\dfrac{\mathrm{Im}\left(\dfrac{V_a - V_b - V_c}{I_a - I_b} + (z_{cc} + z_{Lc})\dfrac{I_c}{I_a - I_b}\right)}{\mathrm{Im}\left(\dfrac{(D - z_{ca})I_a + (E - z_{cb})I_b + FI_c}{I_a - I_b}\right)}$
ABC/ ABCG	$\dfrac{\mathrm{Im}\left(\dfrac{V_b - V_c}{I_b - I_c}\right)}{\mathrm{Im}\left(\dfrac{GI_a + HI_b + JI_c}{I_b - I_c}\right)}$	$\dfrac{\mathrm{Im}\left(\dfrac{V_c - V_a}{I_c - I_a}\right)}{\mathrm{Im}\left(\dfrac{KI_a + LI_b + MI_c}{I_c - I_a}\right)}$

Note: variables and parameters are defined in [24].

The FDEEI is calculated every time a possible faulty section is reported, e.g., at *Step 10* of the algorithm for the downstream system. The lower FDEEI indicates the faulty section.

B. Fault Type Identification

For the calculation of the FDEEI, the fault type should be identified through the voltage and current phasor measurements, i.e., $\boldsymbol{V}_1$ and $\boldsymbol{I}_1$, taken from the main substation. In fact, the fault type is determined by calculating and observing the following quantities from the measurements $\boldsymbol{V}_1$ and $\boldsymbol{I}_1$:

1) The phase-angle difference $\varphi_{Is,21}$ between the superimposed negative- ($\boldsymbol{I}_1^{2,s}$) and positive-sequence ($\boldsymbol{I}_1^{1,s}$) current phasors.

2) The phase-angle difference $\varphi_{Is,20}$ between the superimposed negative- ($\boldsymbol{I}_1^{2,s}$) and zero-sequence ($\boldsymbol{I}_1^{0,s}$) current phasors.

3) The phase-angle difference $\varphi_{V,21}$ between the negative- ($\boldsymbol{V}_1^2$) and positive-sequence ($\boldsymbol{V}_1^1$) voltage phasors.

4) The phase-angle difference $\varphi_{V,20}$ between the negative- ($\boldsymbol{V}_1^2$) and zero-sequence ($\boldsymbol{V}_1^0$) voltage phasors.

Table III shows the range of phase-angle differences for each fault type [25].

TABLE III
Range of Phase-angle for Each Fault Type

Fault type	$\varphi_{Is,21}$ (°)	$\varphi_{Is,20}$ (°)	$\varphi_{V,21}$ (°)	$\varphi_{V,20}$ (°)
AB	45 - 75		180 - 300	
BC	165 - 195		−60 - 60	
CA	−75 - −45		60 - 180	
ABG	45 - 75	90 - 150	180 - 300	30 - 150
BCG	165 - 195	−30 - 30	−60 - 60	−90 - 30
CAG	−75 - −45	210 - 270	60 - 180	150 - 270
AG	−15 - 15	−30 - 30	150 - 270	−90 - 30
BG	105 - 135	210 - 270	−90 - 30	150 - 270
CG	225 - 255	90 - 150	30 - 150	30 - 150

VI. Implementation Aspects

Figure 5 illustrates the flowchart of the proposed method. Figure 6 shows the implementation scheme of this method. FL is the abbreviation of fault locator, which is a dedicated substation computer executing the fault location algorithms addressed in this paper.

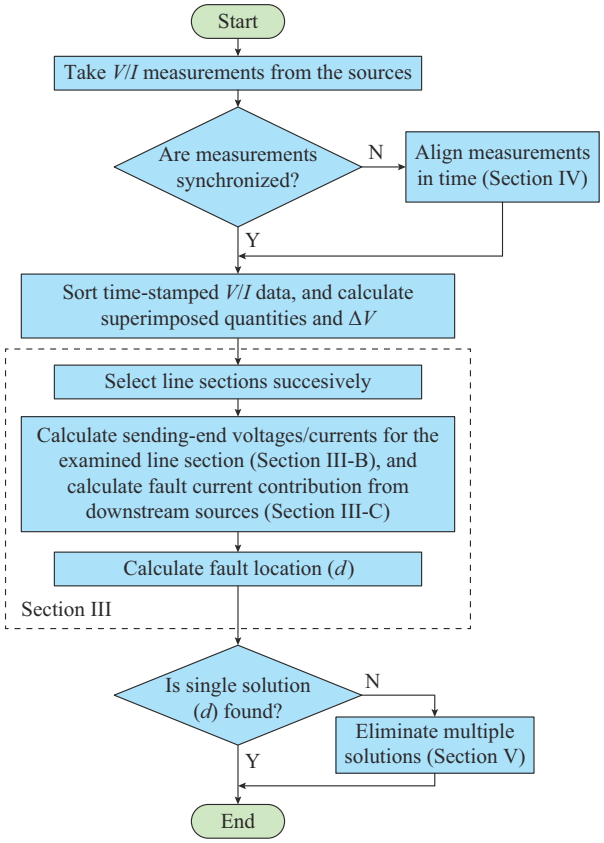

Fig. 5. Flowchart of proposed method.

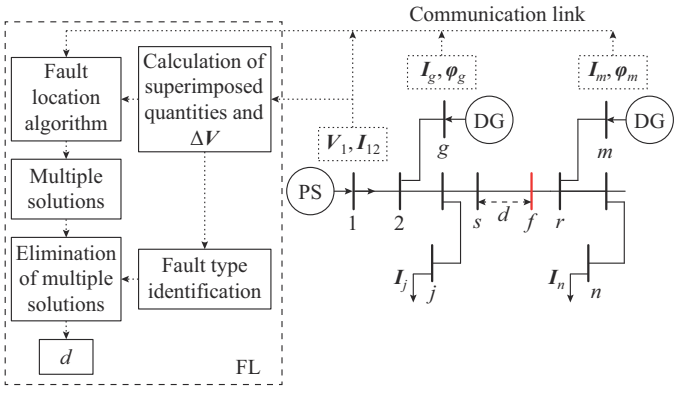

Fig. 6. Implementation scheme.

The required voltage and current phasors are gathered on this substation computer. As already addressed in the previous sections, these phasors may be time-stamped or not. If synchronized phasors are available or desirable, then measurement devices such as micro phasor measurement units (μPMUs) should be utilized. These devices will provide time-stamped voltage/current phasors with a common time reference like that determined by the global positioning system (GPS). If no synchronization means are available or desirable, then voltage/current phasor measurements are locally collected and asynchronously sent to the FL. The FL will artificially align the phasors in time by following the methodology described in Section IV.

We emphasize here that no voltage/current measurements are required from any other point along the feeder. Only phasor measurements from the sources (i.e., from the main substation and the connected DG units) are required. In actual power distribution network, it is impossible to find a DG power plant without voltage and current measurement devices. Voltage and current measurements are required to implement the protection system of the generation units. Moreover, voltage and current measurements are required to measure the active/reactive power produced by the unit at the point of connection with the distribution system for regulatory and/or financial reasons. The same is true for the main substation. In addition, it is impossible that voltage/current sensors are unavailable in the main high-voltage/medium-voltage (HV/MV) power distribution substation for similar reasons.

In addition, it must be emphasized that the proposed method is not designed as a real-time application. Low-speed data communications can be applied for data gathering, which significantly differs from communication channels used for real-time applications. Moreover, the fault location is considered to run offline, just after a fault occurs in the distribution system. Hence, although fault location time is important for service restoration and we are interested in developing a time-efficient method, there are always different time requirements compared with those for fault protection.

VII. Fault Location Results

A modified version of the IEEE 123-bus test distribution feeder model, as shown in Fig. 7, is considered for the simulation studies [26]. In this model, the voltage regulators are removed, whereas the only cable lateral 63-70 has been replaced by an overhead line. Four DG units are connected to buses 31, 54, 87, and 99. The sources connected to buses 31 and 54 are CIDG units, modeled as in [8], while those connected to buses 87 and 99 are synchronous-machine-based units modelled as Thevenin-based DGs.

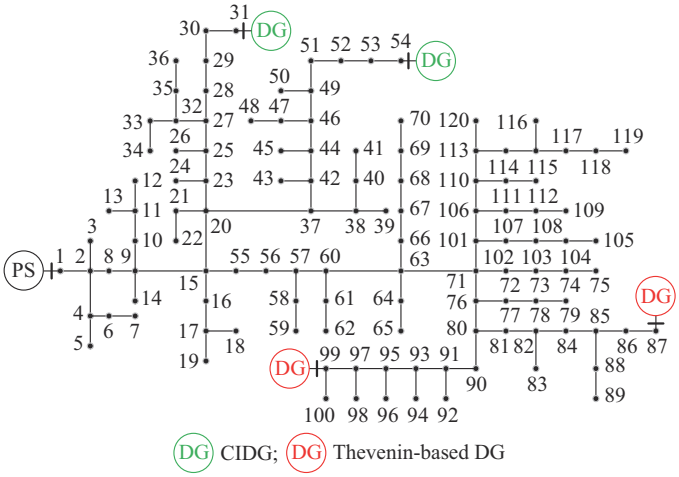

Fig. 7. Modified IEEE 123-bus test distribution feeder model.

The performance of the proposed method is evaluated with the aid of the fault distance estimation accuracy error (FDEAE):

$$FDEAE = \left| d_a - d_m \right| \times 100\% \tag{47}$$

where d_a is the actual fault distances.

The elimination methodology for multiple solutions is evaluated based on how reliably the FDEEI performs, i.e., how often a false section is identified.

A. Performance Evaluation

First, we evaluate the performance of the proposed method for solid faults and synchronized phasor measurements. More complex conditions will be investigated next.

To this end, all common fault types are simulated on different line sections and locations. The proposed method is applied for each simulated fault scenario. Due to space limitations, indicative results are shown in Table IV. Specifically:

1) In the first column of Table IV, the actual faulty section and fault distance d_a, as well as the length of the examined line section, are presented.

2) In the second column, the considered fault type is shown.

3) The solutions d_m and d_e ($e = 1, 2$) resulting from the main and the extra fault location equations, respectively, are shown in the next three columns of Table IV.

4) The FDEEI and FDEAE are included in the last two columns of Table IV. It is noted that when multiple possible faulty sections are estimated, the bolded values indicate the finally estimated faulty line section (based on the FDEEI) and the exact fault distance.

The results of Table IV show that the FDEEI correctly identifies the actual faulty section in almost all cases. In fact, among all the examined cases (250 in total), there are only three fault scenarios shown in Table IV, i.e., 90-91/0.4/137.16/AB, 90-91/0.4/68.58/ABCG, and 113-120/0.3/304.8/AB, where FDEEI wrongly identifies the faulty section. This is a really great performance considering the multi-branch nature and size of the test feeder.

Moreover, the calculated FDEAE is low, clearly demonstrating the high accuracy of the proposed method. Generally, larger values of FDEAE are calculated at the shortest line sections. For the longest line section 113-120, which is also the remotest, the FDEAE is extremely low.

Since a significant dependence between the FDEAE and the line section length arises, to investigate deeper the accuracy of the proposed method, we calculate the mean value of the FDEAE with respect to different line section lengths. For this purpose, solid faults of all types are considered in the middle of 50 different line sections. Table V presents the mean value of FDEAE as calculated for four different line section lengths. The titles in the last four columns are the line section length/number of lines in each class. For the shortest line section, a maximum error of 2.43% is observed, whereas for line sections with a length in the range of 76.2-228.6 m, the error is in the order of 1.5%. In general, the accuracy is satisfactory for all line section lengths.

TABLE IV
FAULT LOCATION RESULTS

Faulty section/d_a/section length (m)	Fault type	Estimated faulty sections	Estimated fault position			FDEEI (%)	FDEAE (%)
			d_m	d_1	d_2		
90-91/0.4/137.16	AG	82-84	0.8886	0.5413	0.3287	0.5104	0.83
		90-91	**0.4083**	0.4138	0.4320	**0.0486**	
		103-104	0.8743	0.0089	0.0124	0.9878	
		113-120	0.2189	0.1989	0.1880	0.1164	
	AB	69-70	0.6790	0.1798	0.0952	0.7975	1.63
		82-84	0.8240	0.4485	0.3793	0.4977	
		90-91	**0.3837**	0.3462	0.3195	0.1325	
		103-104	0.5908	0.5739	0.4874	**0.1018**	
		113-120	0.2262	0.7159	0.6834	2.0931	
	ABG	82-84	0.8416	0.6953	0.6482	0.2019	1.42
		90-91	**0.3858**	0.3582	0.3532	**0.0780**	
		103-104	0.7455	0.7023	0.6782	0.0741	
		113-120	0.1765	0.0932	0.0025	0.7288	
	ABC	**90-91**	**0.4074**	0.4162	0.4209	**0.0273**	0.74
		113-120	0.2360	0.3154	0.3378	0.3840	
	ABCG	82-84	0.8874	0.6742	0.7194	0.2148	1.97
		90-91	**0.3803**	0.3783	0.3449	0.0995	
		103-104	0.7199	0.6742	0.6563	**0.0759**	
		113-120	0.2001	0.4290	0.4863	1.2869	
113-120/0.3/304.8	AG	84-85	0.0264	0.1906	0.1455	5.3655	0.95
		90-91	0.5817	0.4385	0.4104	0.2703	
		104-105	0.0439	0.1348	0.1276	1.9886	
		113-120	**0.2905**	0.3212	0.3109	**0.0878**	
	AB	69-70	0.8736	0.5586	0.5168	0.3845	0.35
		82-84	0.9716	0.6173	0.5873	0.3801	
		90-91	0.4320	0.3956	0.3682	**0.1160**	
		104-105	0.4355	0.6521	0.7632	0.6249	
		113-120	**0.2965**	0.2641	0.2407	0.1488	
	ABG	90-91	0.5917	0.6400	0.6173	0.0624	0.06
		104-105	0.0402	0.3193	0.5632	9.9764	
		113-120	**0.3006**	0.3054	0.2883	**0.0509**	
	ABC	90-91	0.5489	0.4193	0.4297	0.2357	0.16
		104-105	0.0291	0.7391	0.8621	26.512	
		113-120	**0.2984**	0.3093	0.3103	**0.0382**	
	ABCG	90-91	0.5702	0.2903	0.3683	0.4225	0.18
		104-105	0.0258	0.4721	0.4316	16.513	
		113-120	**0.2982**	0.2917	0.3023	**0.0295**	
93-95/0.5/68.58	AG	85-86	0.5371	0.6406	0.8402	0.3785	2.27
		93-95	**0.5227**	0.5572	0.4963	**0.0583**	
		82-83	0.3572	0.4738	0.4194	0.2503	
		113-120	0.5897	0.5471	0.5603	0.0610	
	AB	82-83	0.7528	0.1998	0.0743	0.8179	3.12
		85-86	0.6238	0.5952	0.6376	0.0340	
		93-95	**0.5312**	0.5462	0.5274	**0.0177**	
		113-120	0.6783	0.3865	0.8753	0.3603	
	ABG	85-86	0.4532	0.7535	0.8637	0.7842	2.56
		93-95	**0.4744**	0.4582	0.4532	**0.0394**	
		103-104	0.5467	0.6054	0.5692	0.0743	
		110-113	0.3982	0.2784	0.7654	0.6115	
	ABC	82-84	0.0231	0.0193	0.0694	1.0844	2.38
		93-95	**0.5238**	0.4976	0.5672	**0.0664**	
		101-106	0.9721	0.7823	0.8725	0.1489	
		103-104	0.3476	0.5432	0.0675	0.6843	
	ABCG	85-86	0.0954	0.1474	0.6521	3.1903	2.16
		93-95	**0.4784**	0.4742	0.4489	**0.0352**	
		103-104	0.0432	0.0542	0.0998	0.7824	
		113-120	0.3721	0.4582	0.5783	0.3928	

B. Sensitivity Analysis

Sensitivity analysis is made for the case leading to the largest FDEAE between all the examined cases, that is, the case of a fault in the middle ($d = 0.5$ p.u.) of section 93-95.

TABLE V
MEAN VALUE OF FDEAE

Fault type	Mean value of FDEAE (%)			
	1-250/5	250-500/5	500-750/55	750-1000/5
AG	1.56	1.39	1.21	0.75
AB	2.43	1.83	1.69	1.27
ABG	2.28	1.82	1.75	1.31
ABC	1.16	0.88	0.73	0.45
ABCG	1.29	0.72	0.59	0.37

TABLE VI
EFFECT OF SYNCHRONIZATION ERRORS ON FDEAE

Faulty section/ d_a/section length (m)	Fault type	FDEAE with different (δ_{31}, δ_{54}, δ_{87}, δ_{99}) (%)			
		(0, 0, 0, 0)	(1.8°, 3.6°, 5.4°, 7.2°)	(9.0°, 10.8°, 12.6°, 14.4°)	(3.0°, 12.1°, 31.2°, 23.4°)
93-95/0.5/ 68.58	AG	2.27	2.27	2.27	2.27
	AB	3.12	3.12	3.12	3.12
	ABG	2.56	2.56	2.56	2.56
	ABC	2.38	2.38	2.38	2.38
	ABCG	2.16	2.16	2.16	2.16

1) Effect of Fault Resistance

In order to investigate the impact of fault resistance on FDEAE, the ground and phase faults with different fault resistances are examined.

Please note that the Greek distribution system operator considers a maximum of 40 Ω for ground faults in short-circuit studies. 40 Ω is also the maximum fault resistance magnitude adopted worldwide in protection design studies as stated in [27]. Moreover, for typical medium-voltage overhead pole configurations, the maximum possible fault resistance is in the order of 10 Ω. Hence, in this paper, neutral-to-ground fault resistances in the range of 0-50 Ω are considered for ground faults. For phase faults, inter-phase fault resistances between 1 Ω and 10 Ω are considered.

From the results in Fig. 8, it is evident that as the fault resistance increases, the FDEAE also increases for all fault types. It is also shown that ground faults are less affected from fault resistance compared with phase faults. In all cases, the FDEAE remains below 7% for any fault type and fault resistance, which is a quite acceptable performance.

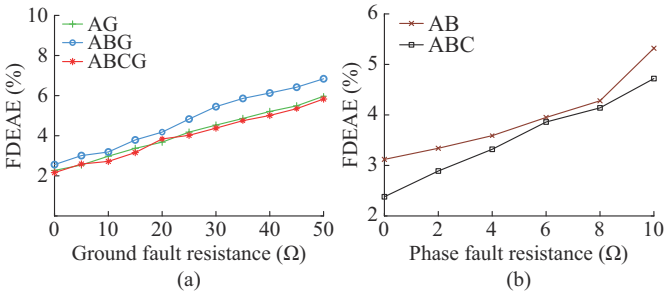

Fig. 8. Effect of fault resistance on FDEAE. (a) Ground fault. (b) Phase fault.

2) Effect of Synchronization Errors

We assume that the voltage phasors measured at source buses 31, 54, 87, and 99 have a synchronization error which is given by the error angles ($\delta_{31}, \delta_{54}, \delta_{87}, \delta_{99}$), respectively, as shown in Table VI. The results clearly show that the performance of the proposed method is practically insensitive to synchronization errors.

3) Effect of Load Variation

A uniform decrease/increase of all load impedances, corresponding to a load variation up to 25% with respect to the initial power consumption, is considered. Figure 9(a) shows that a pre-fault load variation certainly influences the accuracy of the proposed method. For the worst case of 25% load variation, FDEAE does not exceed 10.5%.

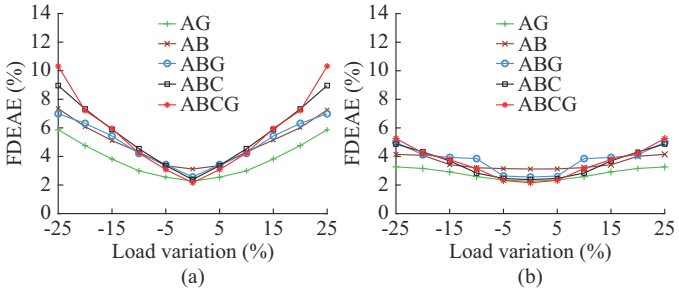

Fig. 9. Effect of load variation on FDEAE. (a) Uncompensated load. (b) Compensated load.

Since this error is relatively large, we consider following the load compensation method in [28].

This method uses measurements taken from the substation to calculate a load factor, which is used to compensate the loads in the calculations. With this method, the FDEAE remains below 5.3% for all fault types (Fig. 9(b)), which is a quite acceptable value.

4) Effect of Measurement Errors

The proposed method utilizes the during-fault voltage and current measurements from the substation (bus 1), as well as the during-fault current and power factor angle measurements from all the DG sources.

To evaluate the performance of the proposed method under measurement errors, seven different measurement error scenarios (scenario 1-7) are considered. Scenario 1 refers to the case without any measurement error in the signals. Table VII shows the phasor magnitude variation for each scenario. The calculated FDEAE is illustrated in Fig. 10, which certainly increases under such errors. However, the algorithm still responses reliably.

TABLE VII
PHASOR MAGNITUDE VARIATIONS FOR EACH SCENARIO

Scenario	Phasor magnitude variations (%)				
	V_1 and I_1	I_{31}	I_{54}	I_{87}	I_{99}
1	0	0	0	0	0
2	+1	0	0	0	0
3	+3	0	0	0	0
4	+5	0	0	0	0
5	+1	−1	−1	−1	−1
6	+3	−1	−1	−1	−1
7	+5	−1	−1	−1	−1

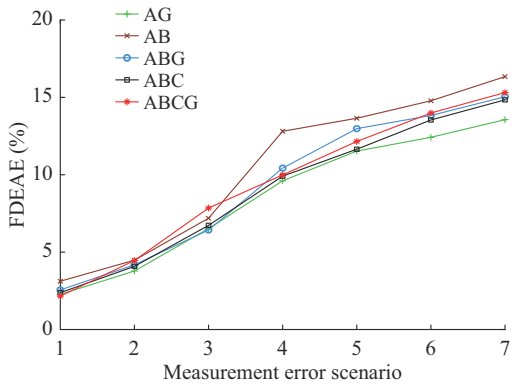

Fig. 10. Effect of measurement error on FDEAE.

5) Effect of Line Parameter Errors

The proposed method utilizes the series line parameters to derive the matrices ***BCBV*** and ***BIBC***. These parameters may change in overhead lines constantly, e.g., due to changes in ambient temperature. For this purpose, we investigate the performance of the proposed method with such line parameter errors.

The IEEE 123-bus test distribution feeder is made up of 11 different overhead line configurations [26]. Table VIII lists the line parameter error scenarios for all overhead line configurations 1-11. Specifically, scenario 1 refers to the line parameters as given in [26], whereas a percentage change on the per-unit length impedance is imposed to all line section configurations in the rest of the scenarios.

TABLE VIII
LINE PARAMETER ERROR SCENARIOS

Scenario	Line impedance variation for line configurations (%)										
	No. 1	No. 2	No. 3	No. 4	No. 5	No. 6	No. 7	No. 8	No. 9	No. 10	No. 11
1	0	0	0	0	0	0	0	0	0	0	0
2	+1	+1	–1	+1	–1	–1	+1	+1	–1	+1	–1
3	+2	–2	+1	+3	–2	+3	–3	+1	+2	–1	+3
4	+3	+4	–2	–3	+3	+4	–2	+3	+3	–4	–2
5	+5	–4	+5	–2	+3	+5	–4	+3	+5	–2	+4

From the results, it is shown that the FDEAE increases as the percentage error in line parameters increases, as shown in Fig. 11. For scenario 5 where the largest line parameter errors are encountered, the FDEAE reaches the maximum value of 9.5%. The latter is acceptable for such a large parameter error.

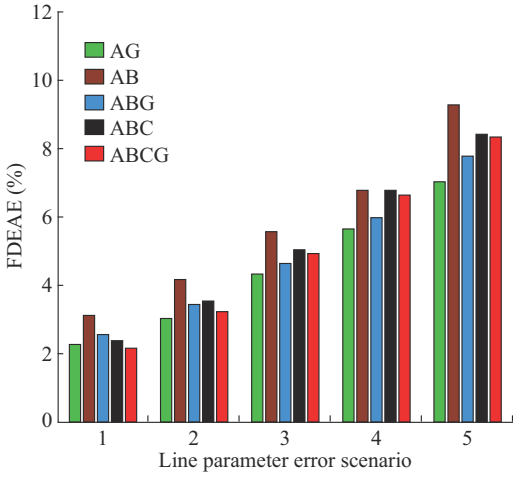

Fig. 11. Effect of line parameter error on FDEAE.

VIII. COMPARISON WITH OTHER METHODS

A. Fault Location Estimation Performance

In this subsection, we compare the proposed method with the methods in [10] and [29]. Reference [10] applies a fault location method that is based on synchronized voltage phasor measurements and the use of monitoring devices along the feeder. Reference [29] applies a time-domain fault location method to find the fault location in distribution systems based on the determination of the line parameters under uncertainty. There are differences between these methods: the method in [10] requires a larger number of monitoring devices, i.e., 16, 21, and 31 devices, and optimization of their locations, which strongly depends on the distribution system examined; whereas the method in [29] does not use fundamental-frequency measurements as our method.

We modified the IEEE 123-bus test distribution feeder to exactly match the pre-/during-fault network conditions (DG production, topology, and fault type/phase/resistance) in [10] and [29]. Tables IX and X depict the comparison results with the methods in [10] and [29], respectively. In Table X, the error equals *FDEAE*/*L*, where *L*=11.8 km is the total feeder length.

TABLE IX
COMPARISON WITH METHOD IN [10]

Fault type	FDEAE with R_f=0.1 Ω (%)		FDEAE with R_f=20 Ω (%)		FDEAE with R_f=50 Ω (%)		FDEAE with R_f=100 Ω (%)	
	Method in [10]	Proposed method	Method in [10]	Proposed method	Method in [10]	Proposed method	Method in [10]	Proposed method
AG	10.92	2.21	5.11	3.89	5.16	5.93	5.14	**7.21**
ABG	7.41	2.30	4.61	4.17	5.21	**6.76**	4.50	**7.58**
AB	9.48	3.17	4.80	**7.15**	4.90	**8.24**	5.17	**9.24**
ABCG	4.86	2.19	4.96	3.92	4.73	**5.89**	4.56	**6.77**

TABLE X
COMPARISON WITH METHOD IN [29]

Location	Fault type	Error with R_f=0 (%)		Error with R_f=0.1 Ω (%)		Error with R_f=1 Ω (%)		Error with R_f=5 Ω (%)		Error with R_f=100 Ω (%)	
		Method in [29]	Proposed method	Method in [29]	Proposed method	Method in [29]	Proposed method	Method in [29]	Proposed method	Method in [29]	Proposed method
1-2	AG	0.261	0.075	0.249	0.075	0.254	0.086	0.263	0.095	0.287	0.170
	ABCG	0.148	0.100	0.149	0.101	0.151	0.122	0.143	0.130	0.164	0.161
	AB	0.198	0.157	0.201	0.159	0.204	0.172	0.210	0.210	0.229	**0.303**
12-14	AG	0.222	0.011	0.228	0.012	0.231	0.030	0.229	0.046	0.236	0.122
	ABCG	0.124	0.072	0.123	0.072	0.123	0.089	0.123	0.099	0.129	0.127
	AB	0.161	0.119	0.161	0.120	0.162	0.151	0.163	0.162	0.169	**0.201**
34-35	AG	0.246	0.071	0.246	0.072	0.247	0.082	0.247	0.097	0.251	0.185
	ABCG	0.181	0.098	0.181	0.099	0.181	0.111	0.182	0.131	0.188	0.179
	AB	0.210	0.144	0.210	0.146	0.210	0.164	0.211	0.198	0.216	**0.222**
70-73	AG	0.223	0.069	0.223	0.070	0.223	0.081	0.223	0.101	0.224	0.209
	ABCG	0.177	0.111	0.177	0.111	0.177	0.124	0.177	0.142	0.181	**0.187**
	AB	0.214	0.151	0.214	0.152	0.214	0.161	0.214	0.195	0.218	**0.235**
99-100	AG	0.281	0.114	0.281	0.117	0.281	0.125	0.281	0.139	0.281	0.199
	ABCG	0.201	0.082	0.201	0.086	0.201	0.097	0.201	0.111	0.202	0.195
	AB	0.255	0.187	0.255	0.205	0.255	0.221	0.255	0.253	0.258	**0.303**
45-47	AG	0.232	0.088	0.234	0.089	0.239	0.100	0.241	0.121	0.260	0.211
	ABCG	0.131	0.102	0.131	0.103	0.131	0.113	0.132	0.128	0.136	**0.198**
	AB	0.176	0.121	0.176	0.123	0.176	0.143	0.176	0.176	0.178	**0.256**

Table IX shows that the proposed method performs better for fault resistances up to 20 Ω, whereas when fault resistance increases, the performance of the method in [10] is better. Table X shows that the proposed method performs better than the method in [29] in most cases. Only for a large fault resistance equaling to 100 Ω, there exist some cases (shown with bolded fonts) where the method in [29] outperforms the proposed method in this paper; but still, the fault distance errors are very close.

However, we would like to state at this point that as addressed in Section VII-B-1), the proposed method in this paper is expected to accurately locate phase faults with a fault resistance up to 10 Ω and ground faults with a fault resistance up to 40 Ω. Larger phase fault resistances are not expected, whereas dealing with ground faults with a resistance larger than 40 Ω is a totally different topic in protection, since sensitive earth relays are required for fault clearance while fault location is challenging for high-resistance magnitudes.

B. Computational Performance

One of the main advantages of the proposed method is that the DLF approach in it reduces substantially the computation time. This is clearly shown in Table XI.

IX. CONCLUSION

The DLF approach is modified in this paper to be used in the proposed fault location method for overhead feeders of power distribution networks. Extensive simulation runs conducted for the modified IEEE 123-bus test distribution feeder under various pre-fault network conditions, fault resistances, and measurement errors show the good performance of the proposed method. The results show that the proposed method finds the exact faulty section and the fault distance inside this section accurately. It is also shown that the proposed method is insensitive to the most challenging error factors. The limited number of synchronized measurements required makes this method attractive for practical application.

TABLE XI
COMPUTATION TIME

Fault type	Computation time (s)	
	Basic algorithm	Algorithm for elimination of multiple estimations
AG	2.0527	4.3423
AB	2.0527	4.2612
ABG	2.0527	4.2612
ABC	2.0527	4.2932
ABCG	2.0527	4.2932

REFERENCES

[1] Y. Liao, "Generalized fault location methods for overhead electric distribution systems," *IEEE Transactions on Power Delivery*, vol. 26, no. 1, pp. 53-64, Aug. 2010.

[2] C. G. Arsoniadis, C. A. Apostolopoulos, P. S. Georgilakis *et al*., "A voltage-based fault location algorithm for medium voltage active distribution systems," *Electric Power Systems Research*, vol. 196, pp. 1-11, Jul. 2021.

[3] S. M. Brahma, "Fault location in power distribution system with penetration of distributed generation," *IEEE Transactions on Power Delivery*, vol. 26, no. 3, pp. 1545-1553, Jul. 2011.

[4] R. F. Buzo, H. M. Barradas, and F. B. Leão, "A new method for fault location in distribution networks based on voltage sag measurements," *IEEE Transactions on Power Delivery*, vol. 36, no. 2, pp. 651-662, Apr. 2020.

[5] F. C. L. Trindade, W. Freitas, and J. C. M. Vieira, "Fault location in distribution systems based on smart feeder meters," *IEEE Transactions on Power Delivery*, vol. 29, no. 1, pp. 251-260, Feb. 2014.

[6] M. Majidi and M. Etezadi-Amoli, "A new fault location technique in smart distribution networks using synchronized/nonsynchronized measurements," *IEEE Transactions on Power Delivery*, vol. 33, no. 4, pp. 1358-1368, Dec. 2017.
[7] S. F. Alwash, V. K. Ramachandaramurthy, and N. Mithulananthan, "Fault-location scheme for power distribution system with distributed generation," *IEEE Transactions on Power Delivery*, vol. 30, no. 3, pp. 1187-1195, Nov. 2014.
[8] C. A. Apostolopoulos, C. G. Arsoniadis, P. S. Georgilakis *et al*., "Unsynchronized measurements based fault location algorithm for active distribution systems without requiring source impedances," *IEEE Transactions on Power Delivery*, vol. 37, no. 3, pp. 2071-2082, Jun. 2022.
[9] A. S. Bretas, C. Orozco-Henao, J. Marín-Quintero *et al*., "Microgrids physics model-based fault location formulation: Analytic-based distributed energy resources effect compensation," *Electric Power Systems Research*, vol. 195, Mar. 2021.
[10] H. Sun, H. Yi, F. Zhuo *et al*., "Precise fault location in distribution networks based on optimal monitor allocation," *IEEE Transactions on Power Delivery*, vol. 35, no. 4, pp. 1788-1799, Aug. 2020.
[11] R. Dashti, M. Ghasemi, and M. Daisy, "Fault location in power distribution network with presence of distributed generation resources using impedance based method and applying π line model," *Energy*, vol. 159, pp. 344-360, Sept. 2018.
[12] R. Dashti, M. Daisy, H. R. Shaker *et al*., "Impedance-based fault location method for four-wire power distribution networks," *IEEE Access*, vol. 6, pp. 1342-1349, Nov. 2017.
[13] R. H. Salim, K. R. C. de Oliveira, A. D. Filomena *et al*., "Hybrid fault diagnosis scheme implementation for power distribution systems automation," *IEEE Transactions on Power Delivery*, vol. 23, no. 4, pp. 1846-1856, Nov. 2008.
[14] R. H. Salim, M. Resener, A. D. Filomena *et al*., "Extended fault-location formulation for power distribution systems", *IEEE Transactions on Power Delivery*, vol. 24, no. 2, pp. 508-516, Apr. 2009.
[15] C. Orozco-Henao, A. S. Bretas, R. Chouhy-Leborgne *et al*., "Active distribution network fault location methodology: a minimum fault reactance and Fibonacci search approach," *International Journal of Electrical Power & Energy Systems*, vol. 84, pp. 232-241, Jan. 2017.
[16] C. Orozco-Henao, A. S. Bretas, A. R. Herrera-Orozco *et al*., "Towards active distribution networks fault location: contributions considering DER analytical models and local measurements," *International Journal of Electrical Power & Energy Systems*, vol. 99, pp. 454-464, Jul. 2018.
[17] A. Bahmanyar and S. Jamali, "Fault location in active distribution networks using non-synchronized measurements," *International Journal of Electrical Power & Energy Systems*, vol. 93, pp. 451-458, Dec. 2017.
[18] R. A. F. Pereira, L. G.W. da Silva, M. Kezunovic *et al*., "Improved fault location on distribution feeders based on matching during fault voltage sags," *IEEE Transactions on Power Delivery*, vol. 24, no. 2, pp. 852-862, Apr. 2009.
[19] P. K. Ganivada and P. Jena, "A fault location identification technique for active distribution system," *IEEE Transactions on Industrial Informatics*, vol. 18, no. 5, pp. 3000-3010, May 2022.
[20] H. Mirshekali, R. Dashti, A. Keshavarz *et al*., "A novel fault location methodology for smart distribution networks," *IEEE Transactions on Smart Grid*, vol. 12, no. 2, pp. 1277-1288, Mar. 2021.
[21] W. H. Kersting and D. L. Mendive, "An application of ladder network theory to the solution of three-phase radial load-flow problems," in *Proceedings of IEEE PES Winter Meeting*, New York, USA, Jan. 1976, pp. 1-6.
[22] D. Thukaram, H. M. W. Banda, and J. Jerome, "A robust three phase power flow algorithm for radial distribution systems," *Electric Power Systems Research*, vol. 50, no. 3, pp. 227-236, Jun. 1999.
[23] J. Teng, "A direct approach for distribution system load flow solutions," *IEEE Transactions on Power Delivery*, vol. 18, no. 3, pp. 882-887, Jul. 2003.
[24] G. Morales-Espana, J. Mora-Florez, and H. Vargas-Torres, "Elimination of multiple estimation for fault location in radial power systems by using fundamental single-end measurements," *IEEE Transactions on Power Delivery*, vol. 24, no. 3, pp. 1382-1389, Jun. 2009.
[25] M. A. Azzouz, A. Hooshyar, and E. F. El-Saadany, "Resilience enhancement of microgrids with inverter-interfaced DGs by enabling faulty phase selection," *IEEE Transactions on Smart Grid*, vol. 9, no. 6, pp. 6578-6589, Nov. 2018.
[26] IEEE. (2017, Aug.). IEEE Test Feeder Case. [Online]. Available: http://sites.ieee.org/pes-testfeeders/files/2017/08/feeder123.zip
[27] L. L. Grigsby, *Electric Power Generation, Transmission and Distribution*. Boca Raton, FL, USA: CRC Press, 2012.
[28] M. S. Choi, S. J. Lee, S. I. Lim *et al*., "A direct three-phase circuit analysis-based fault location for line-to-line fault," *IEEE Transactions on Power Delivery*, vol. 22, no. 4, pp. 2541-2547, Oct. 2007.
[29] H. Mirshekali, R. Dashti, H. R. Shaker *et al*., "Linear and nonlinear fault location in smart distribution network under line parameter uncertainty," *IEEE Transactions on Industrial Informatics*, vol. 17, no. 12, pp. 8308-8318, Dec. 2021.

Charalampos G. Arsoniadis received the diploma of electrical and computer engineering and the M.Sc. degree in energy systems and renewable energy sources from the Department of Electrical and Computer Engineering, Democritus University of Thrace, Xanthi, Greece, in 2016 and 2018, respectively. He is now pursuing the Ph.D. degree at the same department. His research interests include fault location and protection in active distribution systems.

Vassilis C. Nikolaidis received the five-year diploma of electrical and computer engineering from the Department of Electrical and Computer Engineering, Democritus University of Thrace, Xanthi, Greece, in 2001, the M.Eng. degree in energy engineering and management from National Technical University of Athens (NTUA), Athens, Greece, in 2002, and the Ph.D. degree of engineering from NTUA, in 2007. Since 2008, he has been working as a Power Systems Consulting Engineer. Currently, he is an Assistant Professor at the Department of Electrical and Computer Engineering, Democritus University of Thrace. His research interests mainly include power system protection, control, stability, and transients.